

- p46448) and the Protein Identification Resource (PIR) [K. E. Sidman, D. G. George, W. C. Barker, L. T. Hunt, *ibid.* **16**, 1869 (1988)] (accession number s18213).
12. The Mo-ligand distances in the reduced form of FDH₊ are as follows: MGD⁸⁰¹S12, 2.1 Å; MGD⁸⁰¹S13, 2.3 Å; MGD⁸⁰²S12, 2.5 Å; MGD⁸⁰²S13, 2.3 Å; and Se, 2.5 Å. In the oxidized form of FDH₊, the Mo-ligand distances are as follows: MGD⁸⁰¹S12, 2.6 Å; MGD⁸⁰¹S13, 2.3 Å; MGD⁸⁰²S12, 2.4 Å; MGD⁸⁰²S13, 2.4 Å; Se, 2.7 Å; and OH, 2.2 Å.
 13. M. J. Axley, A. Böck, T. C. Stadtman, *Proc. Natl. Acad. Sci. U.S.A.* **88**, 8450 (1991).
 14. EPR spectroscopy provided evidence that the formate-derived proton is located in the vicinity of the Mo(V) center and is slowly exchangeable with water; the proton-accepting group is weakly involved in the electronic ground state of the Mo(V) center and is not a direct ligand to Mo (S. V. Khangulov, V. N. Gladyshev, T. C. Stadtman, in preparation).

15. NMR studies of a SeCys²²¹ derivative of subtilisin suggest the presence of a hydrogen bond between the protonated Nε2 of His⁶⁴ and the selenium of SeCys²²¹ [K. L. House, A. R. Garber, R. B. Dunlap, J. D. Odom, D. Hilvert, *Biochemistry* **32**, 3468 (1993)].
16. S. K. Das, D. Biswas, R. Maiti, S. Sarkar, *J. Am. Chem. Soc.* **118**, 1387 (1996).
17. G. N. George, J. Hilton, K. V. Rajagopalan, *ibid.*, p. 1113.
18. M. J. Barber, H. L. May, J. G. Ferry, *Biochemistry* **25**, 8150 (1986).
19. J. Dong *et al.*, in preparation.
20. V. N. Gladyshev *et al.*, *J. Biol. Chem.* **271**, 8095 (1996). The results of EPR studies of reduced and oxidized FDH₊ crystals are consistent with the presence of a [Mo(IV), Fe₄S_{4(ox)}] state and a [Mo(VI), Fe₄S_{4(ox)}] state, respectively.
21. Z. Otwinowski, in *Proceedings of the CCP4 Study Weekend: Data Collection and Processing*, L. Sawyer, N. Isaacs, S. Bailey, Eds. (SERC Daresbury Laboratory, Warrington, UK, 1993), pp. 56–62.
22. *R-AxisIIc Data Processing Software Version 2.1 Instruction Manual* (Rigaku Corp., 1994).

23. *CCP4: A Suite of Programs for Protein Crystallography* (SERC Collaborative Computing Project No. 4, Daresbury Laboratory, Warrington, UK, 1979).
24. T. A. Jones, J.-Y. Zou, S. W. Cowan, M. Kjeldgaard, *Acta Crystallogr. A* **47**, 110 (1991).
25. A. T. Brünger, *X-PLOR Version 3.1, a System for X-ray Crystallography and NMR* (Yale Univ. Press, New Haven, CT, 1992).
26. K. Kraulis, *J. Appl. Crystallogr.* **24**, 946 (1991); D. J. Bacon and W. F. Anderson, *J. Mol. Graphics* **6**, 219 (1988); E. A. Merritt and M. E. P. Murphy, *Acta Crystallogr.* **D50**, 869 (1994).
27. S. V. Evans, *J. Mol. Graphics* **11**, 134 (1993).
28. We thank D. A. Grahame for use of the anaerobic glove chamber and helpful discussions, C. Ogata and staff at HHMI beamline X4A, and Y. Zhang and L. Hannick for help in the synchrotron data collection.

2 August 1996; accepted 14 January 1997

Formation of Actin Stress Fibers and Focal Adhesions Enhanced by Rho-Kinase

Mutsuki Amano, Kazuyasu Chihara, Kazushi Kimura, Yuko Fukata, Nao Nakamura, Yoshiharu Matsuura, Koza Kaibuchi*

The small guanosine triphosphatase (GTPase) Rho is implicated in the formation of stress fibers and focal adhesions in fibroblasts stimulated by extracellular signals such as lysophosphatidic acid (LPA). Rho-kinase is activated by Rho and may mediate some biological effects of Rho. Microinjection of the catalytic domain of Rho-kinase into serum-starved Swiss 3T3 cells induced the formation of stress fibers and focal adhesions, whereas microinjection of the inactive catalytic domain, the Rho-binding domain, or the pleckstrin-homology domain inhibited the LPA-induced formation of stress fibers and focal adhesions. Thus, Rho-kinase appears to mediate signals from Rho and to induce the formation of stress fibers and focal adhesions.

The small GTPase Rho is inactive in its guanosine diphosphate (GDP)-bound form and active in its guanosine triphosphate (GTP)-bound form (1). When cells are stimulated with certain extracellular signals such as LPA, GDP-Rho is believed to be converted to GTP-Rho, which binds to specific targets that mediate its biological functions. Rho participates in signaling pathways that lead to the formation of actin stress fibers and focal adhesions (2). Actin stress fibers are linked to integrins at the inner surface of the plasma membrane through focal adhesions (1, 2). Rho also participates in the regulation of cell morphology (3), cell aggregation (4), cell motility (5), cytokinesis (6), and smooth muscle contraction (7). In budding yeast, RHO1 (a

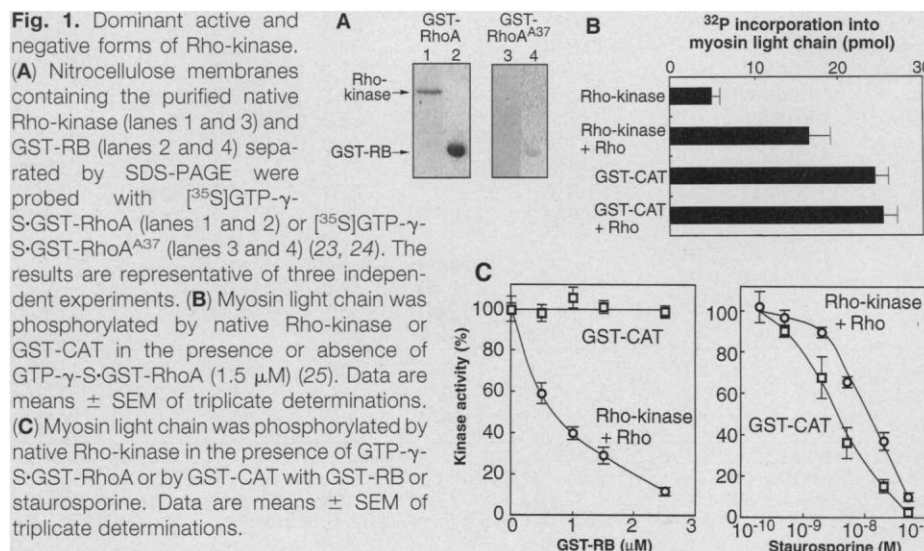
homolog of RhoA) is implicated in the regulation of cell morphology and budding (8). Target proteins, the functions of which are modulated by Rho, include protein kinase N (PKN) (9), Rho-kinase (10) [also called Rho-

binding kinase (11)], and the myosin-binding subunit (MBS) of myosin phosphatase (12). Rho-kinase phosphorylates MBS and consequently inactivates myosin phosphatase (12). Rho-kinase phosphorylates myosin light chain and thereby activates myosin adenosine triphosphatase (ATPase) (13). Other targets of Rho with unknown functions include rhophilin, p160 Rho-associated coiled-coil-containing protein kinase (ROCK), rhotekin, citron (9, 14), and phosphatidylinositol-4-phosphate 5-kinase (PIP5-K) (15). To elucidate the functions of Rho-kinase among these targets of Rho, we produced dominant active and negative forms of Rho-kinase.

Serine-threonine kinases such as protein kinase C (PKC) and Raf are usually composed of regulatory and catalytic domains (16). Deletion of the regulatory domains makes PKC and Raf constitutively active, and the regulatory fragments serve as dominant negative forms of the kinases (17, 18). Rho-kinase is composed of catalytic, coiled-coil, Rho-binding, and pleckstrin-homology domains. We

M. Amano, K. Chihara, Y. Fukata, N. Nakamura, K. Kaibuchi, Division of Signal Transduction, Nara Institute of Science and Technology, Ikoma 630-01, Japan.
K. Kimura, Division of Signal Transduction, Nara Institute of Science and Technology, Ikoma 630-01, Japan, and Second Department of Anatomy, Kyoto University Faculty of Medicine, Kyoto 606, Japan.
Y. Matsuura, Department of Virology II, National Institute of Health, Tokyo 162, Japan.

*To whom correspondence should be addressed.



produced four fragments containing these domains as glutathione-S-transferase (GST) fusion proteins: GST-CAT (catalytic domain, amino acids 6 to 553), GST-COIL (coiled-coil domain, amino acids 421 to 701), GST-RB (Rho-binding domain, amino acids 941 to 1075), and GST-PH (pleckstrin-homology domain, amino acids 1125 to 1388). Guanosine 5'-O-(3-thiotriphosphate) (GTP- γ -S)-GST-RhoA bound to GST-RB, but GTP- γ -S-GST-RhoA^{A37} bound to it very weakly (Fig. 1A). RhoA^{A37} is structurally equivalent to H-Ras^{A35}, which has a mutation in the effector-interacting domain (substitution of threonine to alanine) (1, 19). Rho-kinase had kinase activity on myosin light chain that was activated by GTP- γ -S-GST-RhoA (13), whereas GST-CAT showed full kinase activity without addition of GTP- γ -S-GST-RhoA (Fig. 1B). The molecular activities of Rho-kinase in the presence of GTP- γ -S-GST-RhoA and of GST-CAT in the absence of GTP- γ -S-GST-RhoA were $0.32 \pm 0.02 \text{ s}^{-1}$ and $0.71 \pm 0.02 \text{ s}^{-1}$, respectively, indicating that GST-CAT is constitutively active. GST-CAT mutated at the ATP-binding site (GST-CAT-KD) did not

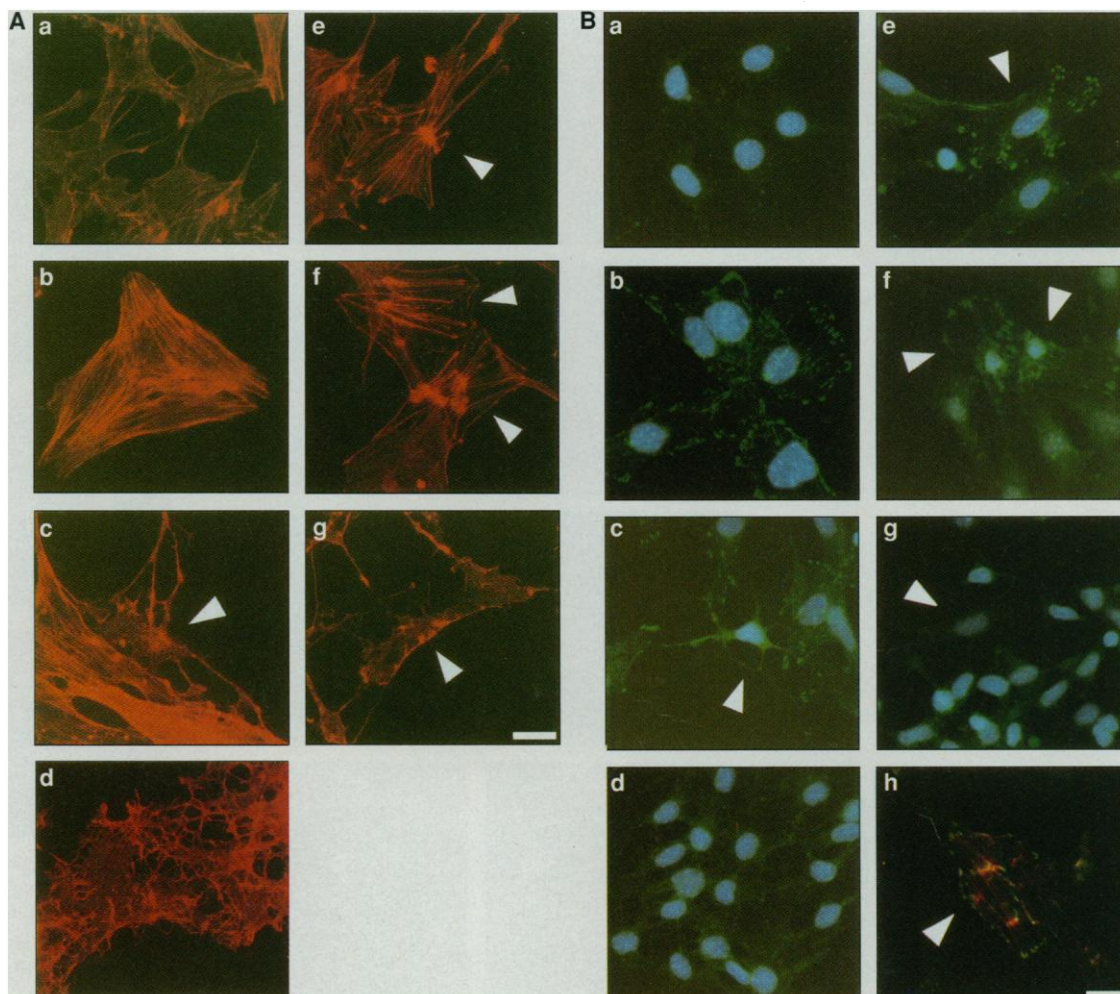
have kinase activity. Although GST-RB inhibited Rho-kinase activity stimulated by GTP- γ -S-GST-RhoA in a dose-dependent manner, it did not affect the kinase activity of GST-CAT (Fig. 1C). The kinase activity of Rho-kinase was not affected by GST-CAT-KD, GST-COIL, or GST-PH (20). The kinase activity of PKN and myosin light chain kinase was not inhibited by GST-CAT-KD, GST-COIL, GST-RB, or GST-PH (20). Rho-induced formation of stress fibers is inhibited by protein kinase inhibitors such as staurosporine (21); staurosporine inhibited the kinase activity of both Rho-kinase and GST-CAT (Fig. 1C).

Confluent, serum-starved Swiss 3T3 cells had very few stress fibers, which were visualized by phalloidin (Fig. 2A) as described (2). When the cells were stimulated with LPA, new stress fibers appeared and increased in number and diameter (Fig. 2A) (2). Microinjection of GST-CAT also induced stress fiber formation, whereas GST-CAT-KD was inactive in this capacity (20). Injected GST-CAT often caused the formation of a large aggregate of actin filaments connected with stress fibers at the central area. Although it is not clear

why hub-like actin filaments were present, they may have resulted from the high contractility of stress fibers induced by injected GST-CAT. When the cells were microinjected with C3 transferase (C3), which causes adenosine diphosphate ribosylation and inhibition of Rho (22), the cells rounded up within 30 min (3, 20). Injected C3 abolished LPA-induced stress fiber formation (Fig. 2A), whereas it did not inhibit GST-CAT-induced stress fiber formation. Coinjection of GST-CAT with C3 prevented the cells from rounding up. Cells stimulated by LPA in the presence of staurosporine showed randomly arranged actin filaments (Fig. 2A) (21), but cells injected with GST-CAT in the presence of staurosporine did not form stress fibers.

Very few focal adhesions, as visualized by an antibody to vinculin, were observed in confluent, serum-starved Swiss 3T3 cells (Fig. 2B) (2). When the cells were stimulated with LPA, new focal adhesions appeared and increased in number (2). Microinjection of GST-CAT induced focal adhesion formation. Longitudinal stress fibers newly synthesized after injection of GST-CAT were linked to focal adhesions that had an elongated arrow-

Fig. 2. Actin reorganization and focal adhesion formation induced by Rho-kinase. **(A)** Actin reorganization caused by Rho-kinase. Actin filaments in confluent, serum-starved Swiss 3T3 cells stimulated by vehicle (a), stimulated by LPA (200 ng/ml) for 15 min without injection (b), microinjected with C3 (80 μ g/ml) and stimulated by LPA (c), stimulated by LPA 15 min after treatment with 100 nM staurosporine (d), microinjected with GST-CAT (0.5 mg/ml) alone (e), microinjected with GST-CAT and C3 (f), and microinjected with GST-CAT 15 min after treatment with staurosporine (g) (26). **(B)** Focal adhesion formation induced by Rho-kinase. Vinculin localization is shown. Images (a) through (g) show the same treatments as in (A), except that actin filaments and vinculin localization are shown in Swiss 3T3 cells microinjected with GST-CAT (h). The arrowheads show the injected cells. Scale bars, 20 μ m.



head shape, as revealed by dual immunofluorescence analysis (Fig. 2B). Thus, it seems clear that GST-CAT-induced focal adhesions exhibit the specific features of adhesions elicited by Rho (21). Microinjection of C3 abolished the LPA-induced formation of focal adhesions, whereas it did not abolish that induced by GST-CAT. Staurosporine inhibited both LPA-induced and GST-CAT-induced formation of focal adhesions. Injection of constitutively active PKN or MBS did not induce formation of stress fibers and focal adhesions, nor did it affect those induced by GST-CAT (20).

Injection of GST-RB or GST-PH inhibited LPA-induced formation of stress fibers and focal adhesions (Fig. 3). About 30% of the cells injected with GST-CAT-KD did not form stress fibers or focal adhesions in the presence of LPA; GST-COIL had no effect. The GST-CAT-induced formation of stress fibers and focal adhesions was not inhibited by injection of GST-CAT-KD, GST-COIL, GST-RB, or GST-PH, which indicated that GST-CAT-KD, GST-RB, and GST-PH inhibited the functions of endogenous Rho-kinase but did not inhibit

the functions of the exogenously overexpressed GST-CAT.

Because Swiss 3T3 cells are not suitable for nuclear injection of plasmids, we examined the morphological effects of Rho-kinase in Madin-Darby canine kidney (MDCK) cells microinjected with cDNAs encoding various domains of Rho-kinase. Microinjection of the cDNA encoding Rho^{V14} into MDCK cells resulted in increased formation of stress fibers (Fig. 4A) and focal adhesions (20, 21). Rho^{V14} is structurally equivalent to H-Ras^{V12} (substitution of glycine to valine) (1, 19). Stress fibers and focal adhesions formed in cells injected with the cDNA encoding CAT (Fig. 4B) (20). The cDNAs encoding CAT-KD, the constitutively active form of PKN, or MBS had no effect. Coinjection of the cDNAs encoding CAT-KD, RB, or PH inhibited Rho^{V14}-induced stress fiber formation (Fig. 4, C to E) and focal adhesion formation. CAT-KD was less effective than RB or PH. COIL was inactive in this capacity.

We assume that CAT behaves as a dominant active form, and that CAT-KD, RB,

and PH behave as dominant negative forms for Rho-kinase but not for CAT. CAT-KD at high concentrations may inhibit interaction of Rho-kinase with substrates such as myosin, as described for other kinases (18). Because the PH domain is supposed to localize molecules at the specified regions, PH may inhibit the proper localization of Rho-kinase in cells. CAT existed in the cytoplasm in MDCK cells, though Rho-kinase is partly localized at cell-to-cell junctions (20). RB may tie up activated Rho and inhibit interaction of Rho with targets such as PKN in addition to Rho-kinase. Consistently, the inhibitory effect of RB could be reversed by overexpression of RhoA^{V14} in MDCK cells, but the inhibitory effect of CAT-KD and PH could not be rescued by overexpression of RhoA^{V14} (20). CAT-KD and PH may serve as more specific inhibitors for Rho-kinase. Taken together, these findings strongly suggest that Rho-kinase regulates the formation of stress fibers and focal adhesions in Swiss 3T3 and MDCK cells in response to activation of Rho. Because the organization of the CAT-induced stress fibers is somewhat different from that induced by LPA in Swiss 3T3 cells, additional signals from Rho or the regulatory domain of Rho-kinase may be necessary for the formation of highly organized stress fibers.

Because injection of CAT slightly in-

Fig. 3. Effect of various forms of Rho-kinase on LPA-induced actin filament reorganization and focal adhesion formation. Confluent, serum-starved Swiss 3T3 cells were microinjected with GST-CAT-KD (2 mg/ml) (A and E), GST-COIL (5 mg/ml) (B and F), GST-RB (5 mg/ml) (C and G), or GST-PH (5 mg/ml) (D and H), and then stimulated with LPA (200 ng/ml) (26). Actin filaments and vinculin localization are shown. The arrowheads show the injected cells. Scale bar, 20 μ m.

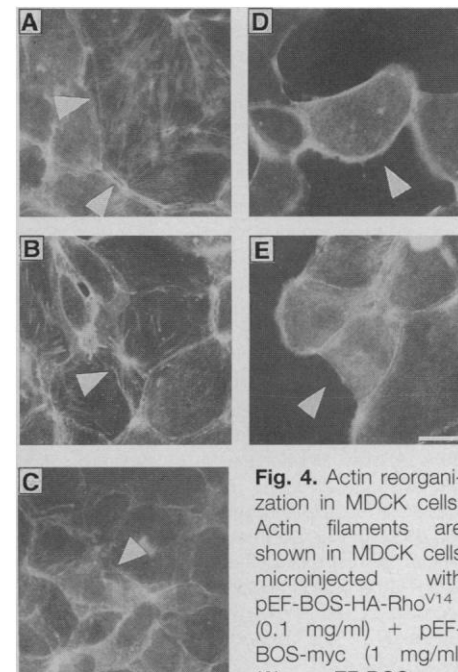
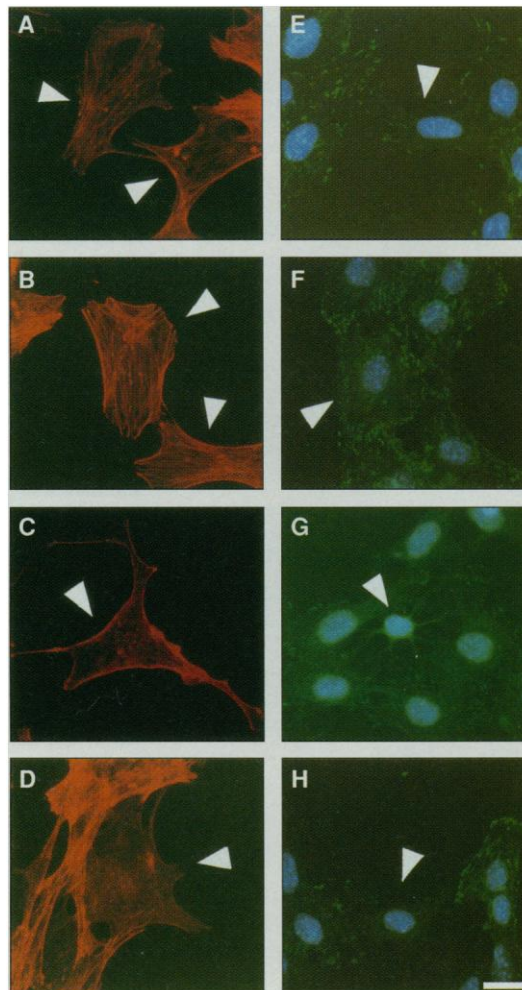


Fig. 4. Actin reorganization in MDCK cells. Actin filaments are shown in MDCK cells microinjected with pEF-BOS-HA-Rho^{V14} (0.1 mg/ml) + pEF-BOS-myc (1 mg/ml) (A), pEF-BOS-myc-CAT (0.1 mg/ml) + pEF-BOS-myc (1 mg/ml) (B), pEF-BOS-HA-Rho^{V14} + pEF-BOS-myc-CAT-KD (1 mg/ml) (C), pEF-BOS-HA-Rho^{V14} + pEF-BOS-myc-RB (1 mg/ml) (D), or pEF-BOS-HA-Rho^{V14} + pEF-BOS-myc-PH (1 mg/ml) (E) (27). The arrowheads show the injected cells. Scale bar, 20 μ m.

creased the intensity of phalloidin staining, Rho-kinase appears to induce actin polymerization to a small extent. The cells stimulated by LPA in the presence of staurosporine showed randomly arranged actin filaments, but the cells injected with CAT in the presence of staurosporine did not form stress fibers, indicating that there are additional pathways (such as PIP5-K) that induce actin polymerization downstream of Rho.

REFERENCES AND NOTES

1. C. Nobes and A. Hall, *Curr. Opin. Genet. Dev.* **4**, 77 (1994); Y. Takai, T. Sasaki, K. Tanaka, H. Nakanishi, *Trends Biochem. Sci.* **20**, 227 (1995).
2. A. J. Ridley and A. Hall, *Cell* **70**, 389 (1992); *EMBO J.* **13**, 2600 (1994).
3. H. F. Paterson *et al.*, *J. Cell Biol.* **111**, 1001 (1990).
4. T. Tomimaga *et al.*, *ibid.* **120**, 1529 (1993).
5. K. Takaishi *et al.*, *Oncogene* **9**, 273 (1994).
6. K. Kishi, T. Sasaki, S. Kuroda, T. Itoh, Y. Takai, *J. Cell Biol.* **120**, 1187 (1993); I. Mabuchi *et al.*, *Zygote* **1**, 325 (1993).
7. K. Hirata *et al.*, *J. Biol. Chem.* **267**, 8719 (1992); M. C. Gong *et al.*, *Proc. Natl. Acad. Sci. U.S.A.* **93**, 1340 (1996).
8. H. Bussey, *Science* **272**, 224 (1996).
9. M. Amano *et al.*, *ibid.* **271**, 648 (1996); G. Watanabe *et al.*, *ibid.*, p. 645.
10. T. Matsui *et al.*, *EMBO J.* **15**, 2208 (1996).
11. T. Leung, E. Manser, L. Tan, L. Lim, *J. Biol. Chem.* **270**, 29051 (1995).
12. K. Kimura *et al.*, *Science* **273**, 245 (1996).
13. M. Amano *et al.*, *J. Biol. Chem.* **271**, 20246 (1996).
14. P. Madaule *et al.*, *FEBS Lett.* **377**, 243 (1995); T. Ishizaki *et al.*, *EMBO J.* **15**, 1885 (1996).
15. L. Chong *et al.*, *Cell* **79**, 507 (1994).
16. Y. Nishizuka, *Nature* **334**, 661 (1988); S. K. Hanks, A. M. Quinn, T. Hunter, *Science* **241**, 42 (1988); U. R. Rapp, *Oncogene* **6**, 495 (1991).
17. K. Kaibuchi *et al.*, *J. Biol. Chem.* **264**, 13489 (1989); S. Hirai *et al.*, *EMBO J.* **13**, 2331 (1994).
18. W. Kolch, G. Heidecker, P. Lloyd, U. R. Rapp, *Nature* **349**, 426 (1991).
19. T. Satoh, M. Nakafuku, Y. Kaziro, *J. Biol. Chem.* **267**, 24149 (1992); F. McCormick, *Curr. Opin. Genet. Dev.* **4**, 71 (1994).
20. M. Amano *et al.*, unpublished data.
21. C. D. Nobes and A. Hall, *Cell* **81**, 53 (1995); A. J. Ridley, P. M. Comoglio, A. Hall, *Mol. Cell. Biol.* **15**, 1110 (1995).
22. K. Aktories, U. Braun, S. Rosener, I. Just, A. Hall, *Biochem. Biophys. Res. Commun.* **158**, 209 (1989); A. Sekine, M. Fujiwara, S. Narumiya, *J. Biol. Chem.* **264**, 8602 (1989).
23. The cDNAs encoding the catalytic domain (amino acids 6 to 553) and catalytic domain mutated at the ATP-binding site (Lys¹²¹ → Gly) were inserted into the Bam HI site of pACYM1-GST to produce GST-CAT and GST-CAT-KD, respectively. GST-CAT and GST-CAT-KD were produced in Sf9 cells with a baculovirus system [Y. Matsuura *et al.*, *J. Gen. Virol.* **68**, 1233 (1987)] and purified on a glutathione-Sepharose column (10). The cDNAs encoding the coiled-coil domain (amino acids 421 to 701), Rho-binding domain (amino acids 941 to 1075), and pleckstrin-homology domain (amino acids 1125 to 1388) were inserted into the Bam HI site of pGEX-2T to produce COIL, RB, and PH, respectively. COIL, RB, and PH were produced and purified from *E. coli* as described (10). The pEF-BOS-myc mammalian expression plasmids encoding CAT, CAT-KD, COIL, RB, and PH were constructed.
24. Binding of Rho to Rho-kinase was determined by overlay assay as described (10). Purified Rho-kinase (0.25 μg) or GST-RB (2.5 μg) were separated on an SDS-polyacrylamide gel (12%), transferred to nitrocellulose membrane, and probed with [³⁵S]GTP-γ-S-GST-RhoA or [³⁵S]GTP-γ-S-GST-RhoA^{A97}. The la-

beled bands were visualized by an image analyzer (Fuji).

25. Rho-kinase activity was assayed in 50 μl of the reaction mixture [40 mM tris-HCl (pH 7.5), 2 mM EDTA, 1 mM dithiothreitol, 6.5 mM MgCl₂, 0.1% 3-[(3-cholamidopropyl)dimethylammonio]-1-propanesulfonic acid, 0.1 μM calyculin A, 100 μM [γ-³²P]ATP (14 to 540 mCi/mmol), 4 μg of myosin light chain, and 20 ng of Rho-kinase or 8 ng of GST-CAT with or without 1.5 μM GTP-γ-S-GST-RhoA (13). After incubation for 10 min at 30°C, the reaction mixtures were boiled in SDS-sample buffer and subjected to SDS-polyacrylamide gel electrophoresis (PAGE). The labeled bands were visualized by an image analyzer (Fuji).
26. Swiss 3T3 cells were cultured in Dulbecco's modified Eagle's medium (DMEM) supplemented with fetal bovine serum (10%). Cells were seeded at a density of 8 × 10³ to 10 × 10³ cells onto 12-mm glass cover slips. After 4 days, the cells were deprived of serum for 24 hours in DMEM. Recombinant proteins were microinjected along with a marker protein (rabbit immunoglobulin G, 1 mg/ml) into the cytoplasm of cells. After microinjection, the cells were incubated at 37°C for 30 min. Actin and vinculin were visualized

by tetramethylrhodamine B isothiocyanate (TRITC)-labeled phalloidin and an antibody to vinculin, respectively, as described (2). Nuclei were visualized by bisbenzimidazole.

27. MDCK cells were cultured in minimum essential medium supplemented with fetal bovine serum (10%). Cells were seeded at a density of 2 × 10³ cells onto 12-mm glass cover slips and cultured for 1 day. Various plasmids were injected into the nucleus as described [A. Ridley *et al.*, *Cell* **70**, 401 (1992)]. After microinjection, the cells were incubated at 37°C for 3 hours. Actin was visualized with TRITC-labeled phalloidin as described (2).
28. We thank M. Ito for chicken myosin light chain, S. Narumiya for C3 transferase, Y. Ono for the PKN cDNA, K. Umeson and R. Yu for critical reading of the manuscript, and M. Nishimura for secretarial assistance. Supported by grants-in-aid for scientific research and for cancer research from the Ministry of Education, Science, and Culture of Japan and by grants from the Mitsubishi Foundation and Kirin Brewery Company.

14 August 1996; accepted 26 December 1996

APC-Mediated Proteolysis of Ase1 and the Morphogenesis of the Mitotic Spindle

Yue-Li Juang, James Huang, Jan-Michael Peters,* Margaret E. McLaughlin, Chin-Yin Tai, David Pellman†

The molecular mechanisms that link cell-cycle controls to the mitotic apparatus are poorly understood. A component of the *Saccharomyces cerevisiae* spindle, Ase1, was observed to undergo cell cycle-specific degradation mediated by the cyclosome, or anaphase promoting complex (APC). Ase1 was degraded when cells exited from mitosis and entered G₁. Inappropriate expression of stable Ase1 during G₁ produced a spindle defect that is sensed by the spindle assembly checkpoint. In addition, loss of Ase1 function destabilized telophase spindles, and expression of a nondegradable Ase1 mutant delayed spindle disassembly. APC-mediated proteolysis therefore appears to regulate both spindle assembly and disassembly.

Cell cycle-specific proteolysis was first discovered as a mechanism for inactivation of mitotic cyclins. B-type cyclins are degraded through the ubiquitin-proteasome pathway (1-3). The cell-cycle specificity of this process comes from the ubiquitination reaction and not from the degradation by the proteasome. Ubiquitination requires the activation of ubiquitin by an E1 enzyme and its subsequent transfer to one of a family of ubiquitin-conjugating enzymes (E2 enzymes). Often, a third activity, the E3, is also required and is a determinant of substrate specificity (1). The E3 for proteolysis

of mitotic cyclins is a multiprotein complex termed the cyclosome or anaphase promoting complex (4-7). Ubiquitination of mitotic cyclins requires a sequence motif termed the destruction box that is thought to be recognized by the APC (2, 8).

Although the role of the APC in cyclin proteolysis is well established, there is now mounting evidence that the APC has other cell-cycle functions. A requirement for the APC during sister chromatid separation was deduced from experiments in *Xenopus laevis* egg extracts and in yeast (5, 9, 10). Recently, two APC substrates required for sister chromatid separation have been identified: Cut2, in fission yeast, and Pds1, in budding yeast (11). A role for the APC in some aspect of DNA replication has also been inferred from the finding that alleles of *Saccharomyces cerevisiae* CDC16 and CDC27 allow more than one complete round of DNA replication during a single cell cycle (12).

We found that the APC regulates the mitotic apparatus by targeting a component

Y.-L. Juang, J. Huang, M. E. McLaughlin, C.-Y. Tai, D. Pellman, Department of Pediatric Oncology, The Dana-Farber Cancer Institute, and Department of Pediatric Hematology, The Children's Hospital, Harvard Medical School, 44 Binney Street, Boston, MA 02115, USA.
J.-M. Peters, Department of Cell Biology, Harvard Medical School, 240 Longwood Avenue, Boston, MA 02115, USA.

*Present address: Research Institute of Molecular Pathology, Dr. Bohr-Gasse 7, A-1030 Vienna, Austria.

†To whom correspondence should be addressed. E-mail: david_pellman@dfci.harvard.edu